Effect of Reaction Parameters on the Structure and Properties of Acrylic Rubber/Silica Hybrid Nanocomposites Prepared by Sol-Gel Technique

Abhijit Bandyopadhyay, Mousumi De Sarkar, Anil K. Bhowmick

Rubber Technology Center, Indian Institute of Technology, Kharagpur-721302, India

Received 24 February 2004; accepted 3 September 2004
DOI 10.1002/app.21382
Published online in Wiley InterScience (www.interscience.wiley.com).

ABSTRACT: The effects of a few reaction parameters, namely, type of solvents, tetraethoxysilane (TEOS)-to-water mole ratio, and temperature of gelation at constant concentration of TEOS (45 wt %) and pH of 1.5 were investigated for acrylic rubber/silica hybrid nanocomposites prepared by sol-gel technique. Infrared spectroscopic studies indicated the maximum silica generation within the system when tetrahydrofuran was used as the solvent for the sol-gel reaction. The distribution of the silica particles (average dimension 100 nm) forming a network type of structure within the composite was confirmed by scanning electron microscopic studies (SEM). The other solvents studied here produced a lower amount of silica because of either high polarity of the solvents (methyl ethyl ketone and dimethyl formamide) or their limited miscibility with water (for ethyl acetate). An increase in the proportion of water caused silica agglomeration. Energy dispersive X-ray analysis (EDAX) silicon mapping also demonstrated the existence of agglomerated silica structures at high TEOS-to-water mole ratio (>2). Higher temperature for gelation of the composites caused the aggregation of silica particles. The uncured composites containing nanolevel (<90 nm) dispersion of silica particles demonstrated slightly higher storage modulus, lower value of tan δ_{max}, and higher glass transition temperature compared to the composites with silica particles of a larger dimension (>2 μm). Improvement in tensile strength and modulus was observed in the uncrosslinked as well as in the crosslinked state (cured by a mixed crosslinking system of hexamethylenediamine carbamate and ammonium benzoate). However, the extent of improvement in strength and modulus for the nanocomposites was higher (247 and 57%, respectively) compared to the microcomposite (150 and 27%, respectively) in the cured state. © 2005 Wiley Periodicals, Inc. J Appl Polym Sci 95: 1418–1429, 2005

Key words: acrylic rubber; silica; sol-gel reaction; organic–inorganic hybrid; nanocomposite

INTRODUCTION

Hybridization is an important and evolutionary route for the growth of a strong polymer-filler interface. One of the most popular and practical approaches to prepare organic–inorganic hybrids is the sol-gel reaction.[1–3] The sol-gel technique with its unique mild processing characteristics can be used to prepare well-controlled hybrid composites.[4–8] The process is executed by the *in situ* hydrolysis and condensation of a precursor inorganic material such as alkoxysilane, which forms silica. Tetraethoxysilane is the most widely practiced metal alkoxide as the silica precursor. Electrostatic interactions between the polar functional groups of the polymer and the residual silanol groups of the silica phase restricts the macrophase separation within the hybrid composites. The sol-gel reaction can be demonstrated as.[9]

Correspondence to: A. K. Bhowmick (anilkb@rtc.iitkgp.ernet.in).

Journal of Applied Polymer Science, Vol. 95, 1418–1429 (2005)
© 2005 Wiley Periodicals, Inc.

$$(OR)_4Si \xrightarrow{H^+/H_2O} (HO)_4Si + 4ROH; \quad R = \text{alkyl groups} \quad (1)$$

Step I (Hydrolysis)

$$(HO)_3Si—OH + HO—Si(OH)_3 \xrightarrow{-H_2O} (HO)_3Si—O—Si(OH)_3 \quad (2)$$

Step II (Polycondensation)

The goal of sol-gel process used is to generate the fine structure and to control its surface and interface during the synthesis.

The dispersion of the inorganic phase into the polymer matrix in the hybrid is mostly at the molecular level, as observed from the earlier work done in our laboratory on acrylic rubber/silica and epoxidized natural rubber/silica organic–inorganic composites.[10,11] The properties of such hybrids strongly depend on the morphology of the inorganic phase, which in turn is related to the nature of the polymer

TABLE I
Characteristics of the Solvents

Solvents	Boiling point (°C)	Density (g/ml)	Solubility in water (g/100 g)	Dielectric constant[a]
N, N-Dimethylformamide (DMF)	153.0	0.94	miscible	36.70
Methyl ethyl ketone (MEK)	79.6	0.80	25.60	18.40
Ethyl acetate (EAc)	77.0	0.81	8.70	6.00
Tetrahydrofuran (THF)	66.0	0.89	30.00	7.60

[a] Taken from the internet site www.bandj.com, dated 13 February 2004.

matrix and the conditions employed in the sol-gel reaction. Previously, it was found that acrylic rubber/silica hybrid nanocomposites produce a chemically noninteractive system, whereas epoxidized natural rubber forms intermolecular hydrogen bonds with the silanol groups in the silica moiety above 40 wt % of tetraethoxysilane loading in the hybrids.[10,11] The sol-gel reaction can also be affected by various parameters, such as the relative amounts of the organic and inorganic components,[12] solvents, the ratio of water to alkoxysilane, pH, and the reaction temperature. However, the authors are not aware of any published article on the influence of the later parameters in such polymeric hybrid composites.

Solvents are used in the sol-gel reaction with the following two advantages: (1) to quench liquid–liquid phase separation during the reaction and (2) to control the concentrations of silicate and water to obtain homogeneous molecular level dispersion. Solvents that can be used are of varying dielectric constants (ε). The ε value generally demonstrates the polarity of the solvents, with polar solvents having higher dielectric constant. It has been observed that change in polarity of the solvents affects the rates of hydrolysis and condensation of the alkoxysilane.[13,14] As water is the reactant in the hydrolysis step and the byproduct in the condensation reaction for alkoxysilanes, as shown in eqs. (1) and (2), the amount of water present in the system can also affect the properties of the resultant hybrids. Temperature is another influencing parameter for any chemical reaction. Rate of the reaction strongly depends on the reaction temperature and, therefore, can affect the chemistry of the sol-gel process as well.

The present work is a part of an on-going project on nanosilica reinforcement of various polymers by using tetraethoxysilane as the precursor for silica via sol-gel technique.[10–12] Organic–inorganic hybrid nanocomposites based on acrylic rubber and silica have been successfully prepared.[10] The current observations are related to the variation of properties of the acrylic rubber/silica hybrid nanocomposites with the change in solvents, water-to-tetraethoxysilane mole ratio, and the gelling temperature. The pH of the medium was maintained at 1.5. The concentration of tetraethoxysilane was also kept constant at 45 wt % with respect to the acrylic rubber. The above two variations are the subjects of other articles.

EXPERIMENTAL

Materials

Acrylic rubber (ACM, Nipol AR51, density at 25°C = 1100 kg/m^3, Mooney viscosity, ML_{1+4} at 100°C = 51) was obtained from Nippon Zeon Co. Ltd. (Tokyo, Japan). It was reported to have an epoxy cure site and was made from ethyl acrylate monomer. Tetraethoxysilane (TEOS, density = 0.93 kg/m^3) was procured from ACROS Organics (USA). Hexamethylenediamine carbamate (HMDC, DIAK#1) was supplied by Nicco Corporation Ltd. (Shyamnagar, India). Ammonium benzoate (AmBz) was prepared in the laboratory by reacting ammonium hydroxide and benzoic acid in a 1 : 1 molar ratio in a water bath at around 60°C for 30 min. The salt formation was confirmed by Fourier transform infrared spectroscopy (FTIR) as well as by studying its solubility. Deionized water and concentrated hydrochloric acid (laboratory grade) were obtained from indigenous sources. The different solvents tetrahydrofuran (THF), *N,N*-dimethylformamide (DMF), methyl ethyl ketone (MEK), and ethyl acetate (EAc), employed for the current study, were all of laboratory grade. Their characteristics are given in Table I.

Preparation of the hybrid composites by sol-gel technique

Composition of the samples is depicted in Table II. ACM was dissolved in solvents of different characteristics (Table I). The ratio of solvent to rubber was kept constant at 1 : 2 (w/v) within the reaction medium. TEOS and water in the molar proportions of 1 : 2 with 45 wt % TEOS with respect to the rubber[10] was added to the rubber solutions by stirring at room temperature. The pH of the reaction medium was maintained at 1.5 by adding an appropriate amount of concentrated HCl. The mixture was again stirred for 30 min at room temperature for homogenization. The result-

TABLE II
Composition of the Samples

Composite designation	Solvents	TEOS: H_2O (mole ratio)	Gelling time (days)	Gelling temperature (°C)	Appearance of the composites
ACM T	THF	1 : 2	5	25	Transparent
ACM M	MEK	1 : 2	5	25	Transparent
ACM D	DMF	1 : 2	10	25	Transparent
ACM E	EAc	1 : 2	7	25	Partly transparent, partly opaque
ACM W1	THF	1 : 1	5	25	Transparent
ACM W2	THF	1 : 2	5	25	Transparent
ACM W4	THF	1 : 4	6	25	Partly opaque
ACM W6	THF	1 : 6	6	25	More opaque
ACM W8	THF	1 : 8	8	25	Opaque
ACM W10	THF	1 : 10	8	25	Opaque
ACM 50T	THF	1 : 2	2 + 3	50	Partly opaque
ACM 100T	THF	1 : 2	2 + 3	100	More opaque

ant solution was cast over plane glass plate for gelation at room temperature. The designation of the samples and their respective gelling times are reported in Table II.

Variation in the proportions of the moles of TEOS with respect to water in the hybrid composites was carried out by dissolving the rubber in THF at a constant pH of 1.5. The amount of TEOS was also fixed to 45 wt % with respect to the rubber used. The variation in the molar proportion of water and the gelling time of the respective samples are reported in Table II. Appearance of the samples varied from transparent to nearly opaque (Table II). Curatives (HMDC and AmBz) were added to the rubbers, dissolved in THF. The optimum dose of the curatives (2.5 and 1.5 wt % of HMDC and AmBz, respectively, with respect to the rubber) used for ACM was taken from our earlier work.[10] The curatives were added after mixing TEOS, water, and HCl with the rubbers, by stirring at room temperature for 30 min. The resultant solutions were cast over plane glass plates and gelled at room temperature for 5–8 days under controlled conditions. The resultant films were subjected to curing reactions in an oven at 170°C for 30 min. The curing time and temperature were taken from our previous work on acrylic rubber.[10]

ACM dissolved in THF was subjected to react with TEOS and water in molar proportions of 1 : 2 at room temperature, at identical pH, following the procedure mentioned earlier. The cast films were kept for 2 days at room temperature and then allowed to gel separately in an oven for another 3 days at 50 and 100°C. The initial gelation period of 2 days at room temperature was allowed to restrict the formation of pores over the samples by rapid evaporation of solvents and by-products of the hydrolysis and condensation of TEOS.

Characterization of the composite

Infrared spectroscopy (FTIR)

The infrared spectra of the hybrid composite films were recorded with a Nicolet Nexus FTIR spectrophotometer in an ATR mode by using a 45° KRS5 prism at room temperature (25°C). The samples were scanned from 2000 to 600 cm^{-1} with a resolution of 4 cm^{-1}. All spectra were taken after an average of 32 scans for each specimen.

Transmission electron microscopy (TEM)

TEM studies were carried out by using a TEM (model C-12, Philips) on very thin films of uncured hybrid composites, cast directly over the copper grids of 300 mesh size. The acceleration voltage was 120 kV. The images presented in this study were of identical magnifications of ×90,000.

Scanning electron microscopy (SEM)

SEM investigations of the hybrid composites were made by using a JEOL JSM 5800 scanning electron microscope. The sample films were sputter-coated with gold. The operating voltage was maintained at 20 kV and the magnifications used are stated in the caption for the respective images.

EDAX silicon mapping

The dispersion of silica particles in the ACM matrix was observed through X-ray silicon mapping of the hybrid composite, recorded in an Oxford EDAX system attached to the SEM at a magnification of ×2000.

Dynamic mechanical thermal analysis (DMTA)

Dynamic mechanical thermal analysis (DMTA) of the hybrid composite films was done in a DMTA IV

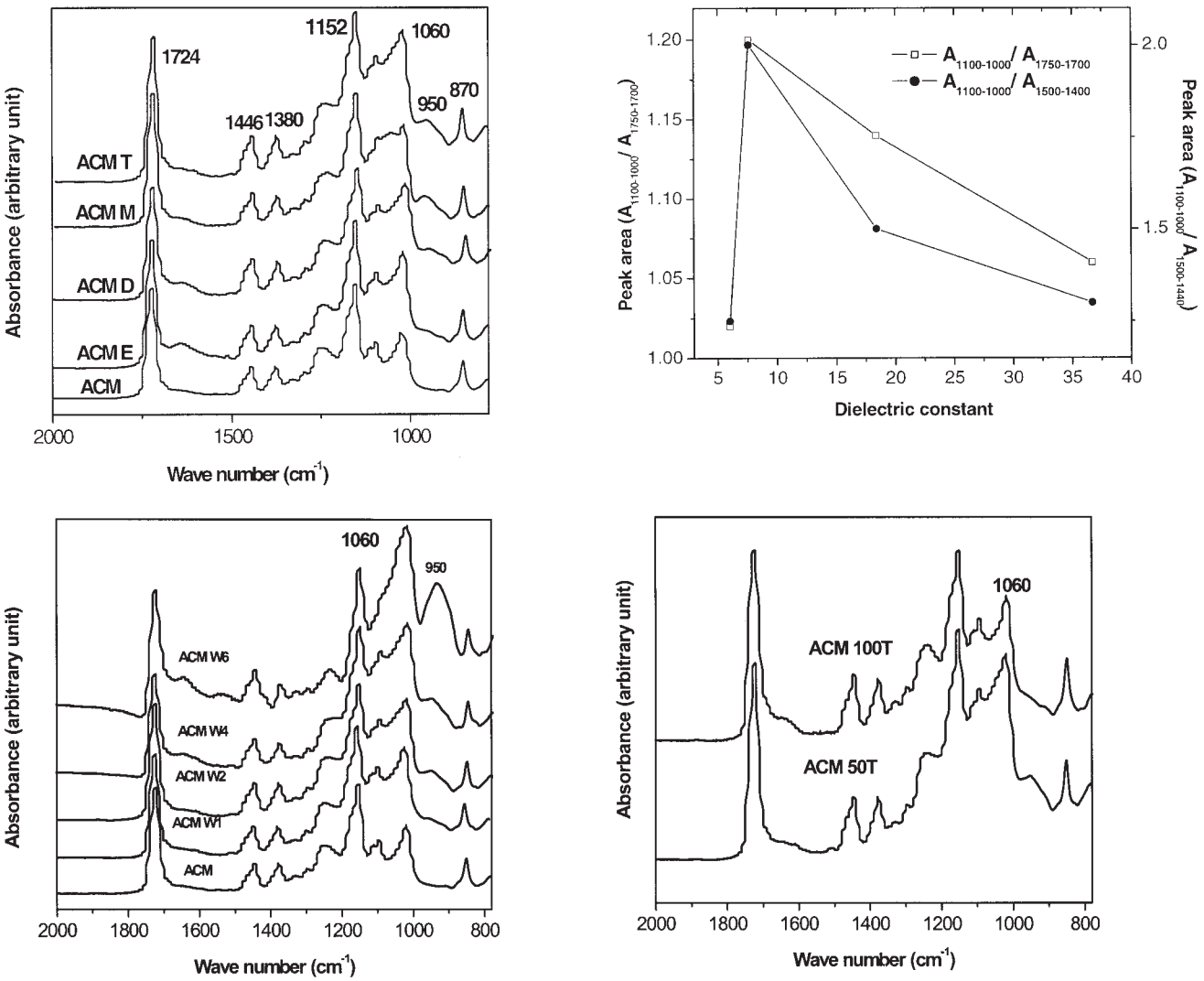

Figure 1 (a) FTIR spectra for the uncured ACM/silica hybrid composites prepared in different solvents. (b) Plot of relative peak absorption area, normalized against the constant absorption intensities of the C═O stretching (1724 cm^{-1}) and C—H bending vibrations (1446 cm^{-1}), in the range of 1100–1000 cm^{-1} for the hybrid composites prepared in different solvents. (c) FTIR spectra for the uncured hybrids prepared by using different TEOS-to-water mole ratios. (d) FTIR spectra for the uncured hybrids prepared by varying the gelling temperature.

TABLE III
Characteristic Absorption Peaks for the Representative Uncured ACM/Silica Organic–Inorganic Hybrid Composites

Peak absorption values (cm^{-1})	Peak assignments
1724	Ester C═O stretching
1446	C—H bending
1380	C—H deformation
1152	Asymmetric C—O—C stretching for ester
	Si—O—Si stretching, symmetric ester
1100–1000	C—O—C stretching
950	Si—O stretching for silanol
870	Epoxy C—O—C ring vibration

(Rheometric Scientific) under tension mode. The experiments were carried out at a frequency of 1 Hz. The measurements were taken from −80 to 100°C at a

TABLE IV
Ash Content Data for the Uncured Hybrid Composites Carried Out at 800°C for 8 h

Composite designation	Ash (wt %)
ACM T	16.0
ACM M	15.0
ACM D	14.0
ACM E	13.5
ACM W2	16.0
ACM W6	17.5
ACM 100T	16.2

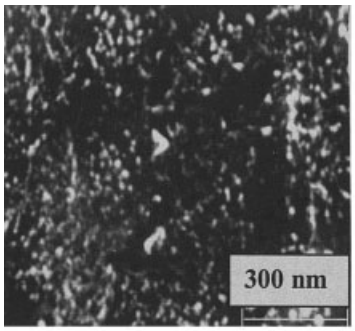

(a)

(b)

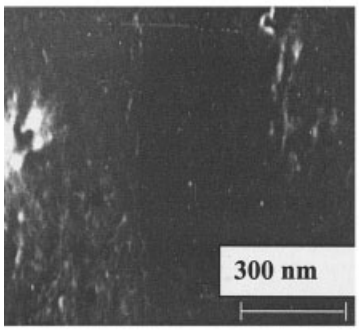

(c)

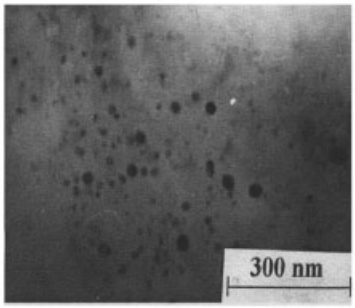

(d)

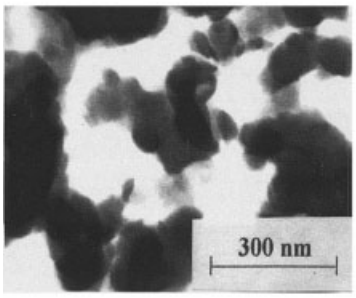

(e)

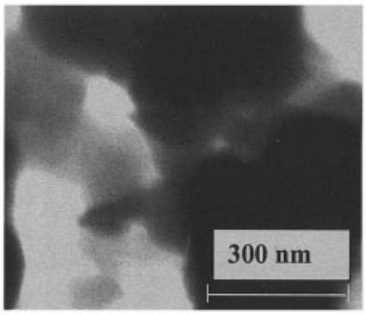

(f)

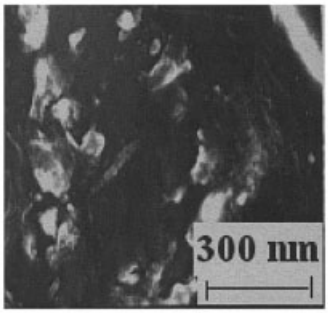

(g)

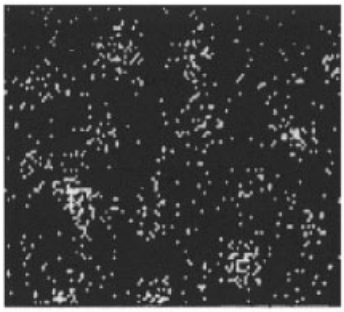

(h)

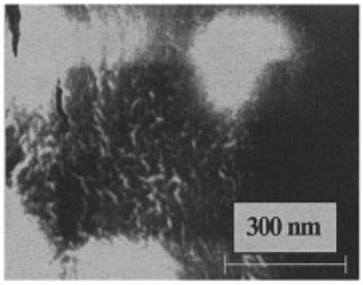

(i)

heating rate of 2°C/min. The data were analyzed by using RSI Orchestrator application software on an ACER computer attached to the machine. The storage modulus and loss tangent (tan δ) were measured for all the samples under identical conditions.

Studies of mechanical properties

The mechanical properties of the composite films were recorded in a universal testing machine (UTM, Zwick 1445) with tensile specimens, punched out from the cast films by using ASTM Die C. The tests were carried out as per ASTM D 412-99 method at 25 ± 2°C at a cross-head speed of 500 mm/min. The average value of three tests was reported for each sample.

Measurement of ash content

The ash content (silica content) of the uncured hybrid composites was measured in a muffle furnace at 800°C for 8 h by pouring the samples in oven-dried silica crucibles. The initial weight of the samples was kept around 2 g and the wt % ash (silica) in the samples was determined by calculating the difference in weights at the start and completion of the test.

RESULTS AND DISCUSSION

Infrared spectroscopic study

Fourier transform infrared spectra (FTIR) for the uncured acrylic rubber/silica organic–inorganic hybrid composites are shown in Figure 1(a–d). The spectrum of the pure rubber sample is also included for the sake of comparison. The corresponding absorption peaks for the specimens are assigned in Table III.

Figure 1(a) exhibits the infrared spectra for ACM/silica hybrid composites (within the region of 2000–600 cm^{-1}), synthesized by using different solvents. The pure rubber gives the characteristic absorptions at 1724 cm^{-1} (C═O stretching), 1446 cm^{-1} (C—H bending), 1380 cm^{-1} (C—H deformation), 1152 cm^{-1} (ester asymmetric C—O stretching), 1040 cm^{-1} (ester symmetric C—O—C stretching), and 870 cm^{-1} (epoxy ring vibration). Strong absorptions due to the Si—O—Si linkages for the silica particles, generated *in situ* within the hybrid composites, appear in the region of 1100–1000 cm^{-1} [Fig. 1(a)]. The absorption band shown in this region may overlap with the symmetric ester C—O—C stretching of the pure ACM. Asymmetric Si—O stretching due to the silanol moieties appear as a weak absorption band around 950 cm^{-1}. A comparative plot of absorption peak area between 1150 and 1000 cm^{-1} [Fig. 1(b)] for the spectra of hybrid composites, normalized against the carbonyl absorption peak at 1724 cm^{-1}, shows the highest absorption intensity due to Si—O—Si linkages in the ACM T hybrid, which reveals the generation of maximum amount of silica in the composite compared to ACM D, ACM E, and ACM M hybrids, at a particular level of TEOS loading (45 wt %). A similar observation is also made when the peak normalization is done with respect to the C—H bending peak for the respective samples [Fig. 1(b)]. The extent of silica generation actually decreases in the order of ACM T > ACM M > ACM D > ACM E. This observation is further supported by the ash content data of the uncured hybrid composites shown in Table IV. ACM D and ACM E virtually show the same amount of silica formation within the system as evident from both Figure 1(b) and Table IV. Close observation in the region around 950 cm^{-1} of the spectra for the uncured ACM/silica hybrid nanocomposites shows that ACM T and ACM M possess similar absorptions at 950 cm^{-1} (Si—O stretching for silanol). ACM D and the ACM E exhibit relatively lower absorptions. This observation indicates that, in ACM T and ACM M, the concentration of silanol moieties, is relatively higher compared to the other hybrid composites.

The FTIR results for the ACM/silica hybrid composites prepared in different solvents clearly suggest that the *in situ* generation of silica through the sol-gel reaction of TEOS in the presence of ACM depends on the characteristic of the solvents. The dielectric constant of the solvents (and polarity) influences the polycondensation reaction of silanol moieties within the reaction medium. When THF is used as solvent, maximum silica formation [Fig. 1(b)] as well as the existence of silanol groups in the nanocomposites [Fig. 1(a)] are evident. It implies that most of the silanol groups have undergone polycondensation reaction in THF to generate the nanosized silica particles, which are dispersed uniformly within the ACM matrix, resulting in transparent composite films. On the other hand, although ACM M possesses a similar concentration of silanol groups [Fig. 1(a)], the extent of polycondensation is lower than that in ACM T, which is evident from the lower absorption in the region of 1100–1000 cm^{-1} because of the presence of silica par-

Figure 2 Photographs of the uncured ACM/silica_hybrid composites. (a) SEM micrograph of ACM T (×10,000). (b) Physical appearance of ACM E (average thickness of the film 0.25 mm). (c) SEM micrograph of ACM E (×10,000). (d) TEM micrograph of ACM W1 (×80,000). (e) TEM micrograph of ACM W4 (×80,000). (f) TEM micrograph of ACM W6 (×80,000). (g) SEM photograph of ACM W6 (×8000). (h) EDAX silicon mapping of ACM W6 (×2000). (i) SEM photograph of ACM 100T (×10,000).

ticles [Fig. 1(b)]. In ACM D, the silica formation is almost comparable with ACM E [Fig. 1(b)]. The silanol concentration of ACM D is higher than that for ACM E. A very high dielectric constant of DMF (Table I) may probably solvate the silanol groups to such an extent that the polycondensation reaction is obstructed. Moreover, the acid–base nature of silanol and DMF (Bronsted Lowry acid and Lewis base) may have played a role in enhancing the silanol–solvent interaction. ACM E exhibits poor silica concentration (and silanol concentration), which may be due to lower solvent–water miscibility (Table I), producing inhomogeneous dispersion of the silica precursors in the medium and causing partial phase separation. Therefore, the FTIR curve for ACM E does not represent the true picture of the composite composition as the silica particles are nonuniformly distributed within the system. Morphological study, discussed in the subsequent section, would provide much information in this regard.

Figure 1(c) sketches the FTIR spectra for pure ACM and the representative ACM/silica hybrid nanocomposites prepared by varying the TEOS-to-water mole ratio of 1 : 1, 1 : 2, 1 : 4, and 1 : 6 in THF at room temperature. When the amount of water is far below the stoichiometric requirement for the hydrolysis of TEOS [1 : 1, eqs. (1) and (2)], the amount of silica generation is least as observed from the peak absorbance at 1060 cm^{-1}. It gradually increases with the proportion of water (1 : 2, 1 : 4, and 1 : 6, TEOS : water). Progressive increase in the absorption peak at 950 cm^{-1} (due to silanol moieties) from lower to higher TEOS-to-water ratio reveals the gradual increase in concentration of the silanol in the hybrids. With the use of excess water from that of the stoichiometric requirement, the initial hydrolysis of TEOS becomes faster, generating a large amount of silanol groups. The excess silanol groups probably form silica agglomerates rather than the nanolevel dispersion within the matrix that is evident from the appearance of the composite films. The composites ACM W1 and ACM W2 are completely transparent but composites prepared with still higher amounts of water (ACM W4-10) are partially transparent to opaque in appearance because of the formation of silica aggregates within the matrix. It is further confirmed from the ash content data for the respective hybrid composites registered in Table IV. Near completion of the hydrolysis reaction of TEOS also leaves some uncondensed silanol groups as is noticed by examining the spectral range from 980 to 900 cm^{-1} [Fig. 1(c)]. Moreover, a higher amount of water delays the gelation time of the hybrids, as evident from Table II.

Figure 1(d) shows the FTIR spectra for the ACM/silica hybrid composites, prepared by gelling the samples at 50 and 100°C. The position of all the peaks discussed earlier remains unchanged; however, the peak absorbance has varied probably because of accelerated silica formation on account of quick removal of water of the condensation reaction of silanol at higher temperature compared to the gelling process carried out under ambient conditions. Enhancement in the rate of condensation causes local agglomeration of silica and the composite appears partially opaque. Higher absorption intensity for the silica particles in the composites gelled at 50 and 100°C may be due to the local agglomeration and generation of higher silica within the ACM matrix.

Morphological observations

Figure 2(a–c) shows the representative micrographs for uncured ACM T and ACM E organic–inorganic hybrid composites. A SEM photograph of ACM T [Fig. 2(a)] exhibits a network type of structure consisting of the spherical silica particles of dimensions of about 90 nm. Because of the dispersion of the silica nanoparticles, optical clarity of the composites is retained. On the other hand, from the visual appearance, ACM E exhibits local agglomeration of silica particles in some places, resulting in inhomogeneous distribution of silica particles. The SEM micrograph of the same composite in Figure 2(c) exhibits very low silica concentration in certain other locations, which supports the nonuniform appearance of the composite film in Figure 2(b). These corroborate the infrared spectroscopic observations of the respective composites.

Figure 2(d–f) are the TEM pictures for the representative ACM/silica uncured hybrid composites, ACM W1, ACM W4, and ACM W6, where the TEOS : water mole ratio is varied. In ACM W1, the size of the silica particles is very small and their average dimension is around 20 nm [Fig. 2(d)]. This is probably due to the scarcity of water for the hydrolysis of TEOS that generates a lower amount of silanol groups, resulting in a lower extent of condensation reaction. Figure 2(e) shows the TEM picture of ACM W4. The size of the black silica particles is distinctly larger than that of ACM W1 [Fig. 2(d)] and is close to 100 nm. The figure demonstrates the existence of discrete silica nanoparticles and also in the aggregated form. The ACM W4 hybrid composite appears partially phase separated in the naked eye due to these agglomerated areas in the figure. A TEM picture of ACM W6 shows the existence of even bigger sized silica particles within the rubber matrix [Fig. 2(f)]. Due to the excess amount of water over the stoichiometric requirement for the hydrolysis of TEOS [eqs. (1) and (2)], the condensation reaction is accelerated to give larger size silica domains in the composite. Beyond ACM W6, the composites show much bigger silica domains and are more phase separated. The SEM photograph of ACM W6 also demonstrates the existence of larger silica particles in the composite [Fig. 2(g)]. The silica clusters are as big as

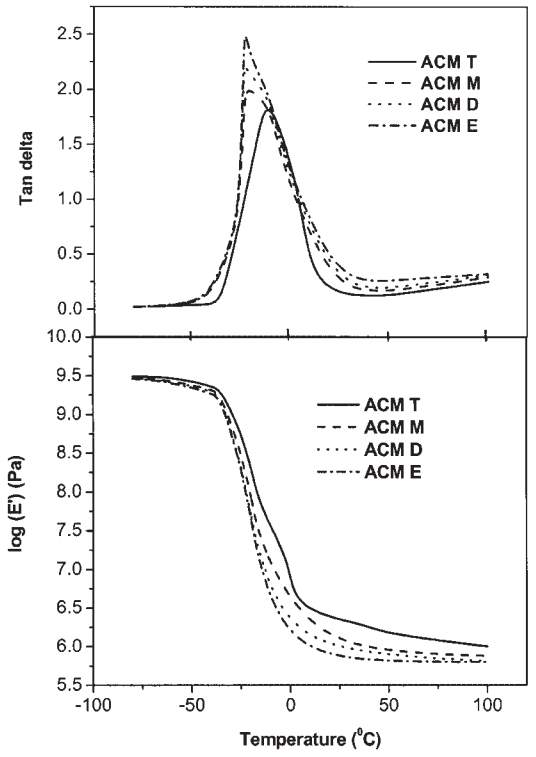

(a)

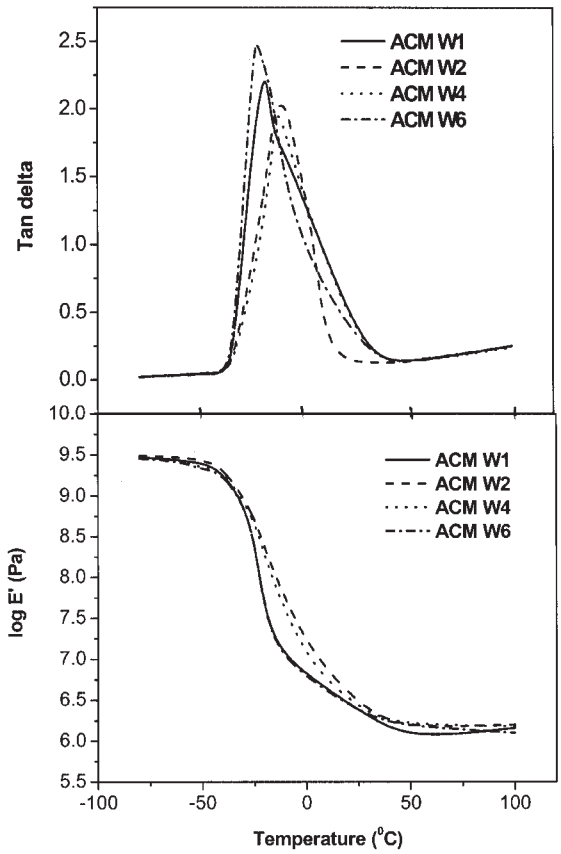

(b)

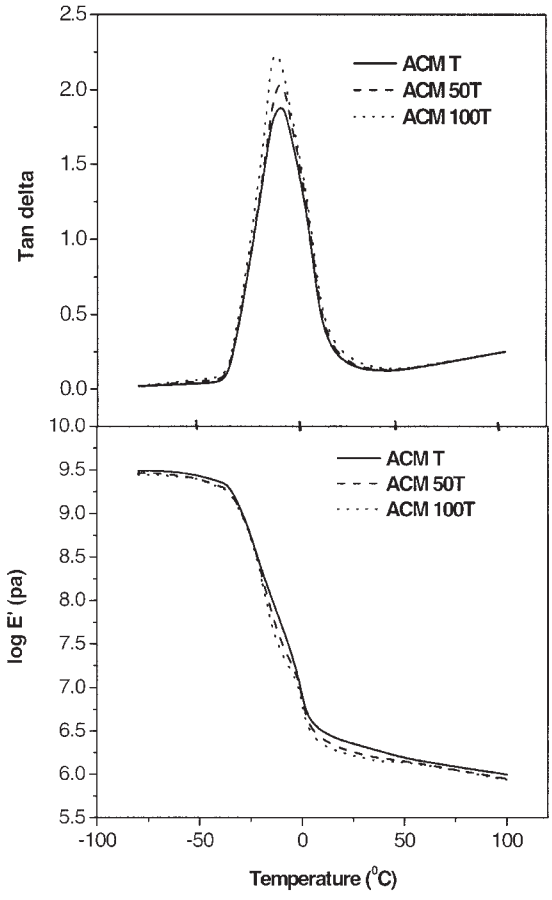

(c)

Figure 3 (a) Storage modulus (log scale) and tan ō plots of uncured ACM/silica hybrid composites prepared with different solvents within the temperature range of −80 to 100°C. (b) Storage modulus values (log scale) and tan δ plots for the uncured hybrid composites prepared by with different TEOS-to-water mole ratios. (c) Storage modulus values (log scale) and tan δ plots for the uncured hybrid composites prepared with varying temperatures.

TABLE V
Storage Modulus, tan ∂_{max}, and the T_g Values for the Uncured Hybrid Composites Obtained from Dynamic Mechanical Analysis

Composite designation	Log E' (PA) −50°C	Log E' (PA) T_g	Log E' (PA) 50°C	tan ∂_{max}	T_g (°C)
ACM T	9.41	7.61	6.20	1.91	−11
ACM M	9.38	7.59	6.15	2.00	−23
ACM D	9.37	7.58	6.11	2.20	−24
ACM E	9.36	7.32	5.98	2.52	−24
ACM W1	9.40	7.26	6.02	2.23	−20
ACM W2	9.41	7.60	6.20	1.91	−11
ACM W4	9.33	7.59	6.20	2.00	−13
ACM W6	9.32	7.56	6.18	2.52	−23
ACM 50T	9.40	7.48	6.17	2.10	−11
ACM 100T	9.40	7.42	6.16	2.30	−13

500 nm and are not strictly spherical in nature. The EDAX mapping of ACM W6 in Figure 2(g) reveals the agglomeration of silicon signals in the sample. The phase-separated silica particles scatters light and renders opacity to the resultant composites. The SEM photographs for ACM 100T [Fig. 2(i)] also exhibits phase-separated morphology of the hybrid composite. Application of heat accelerates the condensation reaction by removing water from the system faster and induces the formation of silica clusters. The samples condensed at 100°C are more opaque than the samples that are condensed at 50°C, because of more effective removal of water from the reaction site at a given time.

Dynamic mechanical thermal analysis

Dynamic mechanical properties demonstrate the viscoelastic nature of the composites. Figure 3 shows the representative storage modulus (log scale) and the loss tangent curves for the uncured ACM hybrid composites in the temperature range of −80 to 100°C. The values of storage modulus at the three different temperatures chosen arbitrarily, and also the peak height values of the loss tangent curves, are given in Table V. The modulus decreases from ACM T to ACM E at −50°C, glass transition temperature (T_g), and 50°C. ACM T possesses uniform dispersion of nanosilica that may impart more elastic nature.[10] Other systems show lower modulus values at these temperatures, which are in line with the lesser extent of silica generation and nonuniform dispersion within the system. The storage modulus values increase marginally for ACM W2 from ACM W1, as the former generates more nanosilica than the latter, as evident from the FTIR data. ACM W4 shows lower modulus value at −50°C compared to ACM W2, but becomes almost same around T_g and above the T_g of the composite. ACM W6, as anticipated, displays lower modulus values, possibly because of agglomerated silica structures that provide lower surface area for the polymer–silica interaction in the composite. When the temperature of condensation is increased, there are no significant changes in the modulus values of the hybrid composites.

The concept of polymer–filler interaction is best illustrated by studying the loss tangent characteristics of the hybrid composites. Table V shows the variation in tan δ peak height values of the uncured ACM/silica hybrid composites. The peak height of the loss tangent curve indicates the chain flexibility of the polymer molecules that undergo resonance with the externally applied sinusoidal stress. The more flexible the chains are, the lesser the polymer–filler interaction would be and the higher the amplitude of vibration would be. Therefore, the peak height of the curves would increase. If the filler interacts with the polymer, the peak height decreases. Therefore, the peak height values of the loss tangent curves of the hybrid composites could be a useful tool in determining the extent of reinforcement offered by the silica particles.

ACM T shows minimum tan δ_{max}, whereas ACM E shows the maximum value (Table V). The result is in line with the amount of silica generated within the system. The nature of variation in tan δ peak height values with the change in proportion of water of the hybrid composites follows the trend of silica particle size distribution within the system (Table V). It first decreases for ACM W2 and then shows a steady increase that reveals low ACM–silica interaction by increasing the proportion of water. Temperature has a similar effect, as it controls the particle size of silica in the hybrids. Nanolevel dispersion of silica particles gives a lower value of the tan δ_{max}, which increases steadily by increasing the temperature due to the increase in the size of the silica particles. Table V reports the T_g values of the hybrid composites. More reinforced structure (illustrated by slightly higher modulus and low tan δ_{max}) exhibits positive T_g shifting, due probably to more effective polymer–filler interactions.

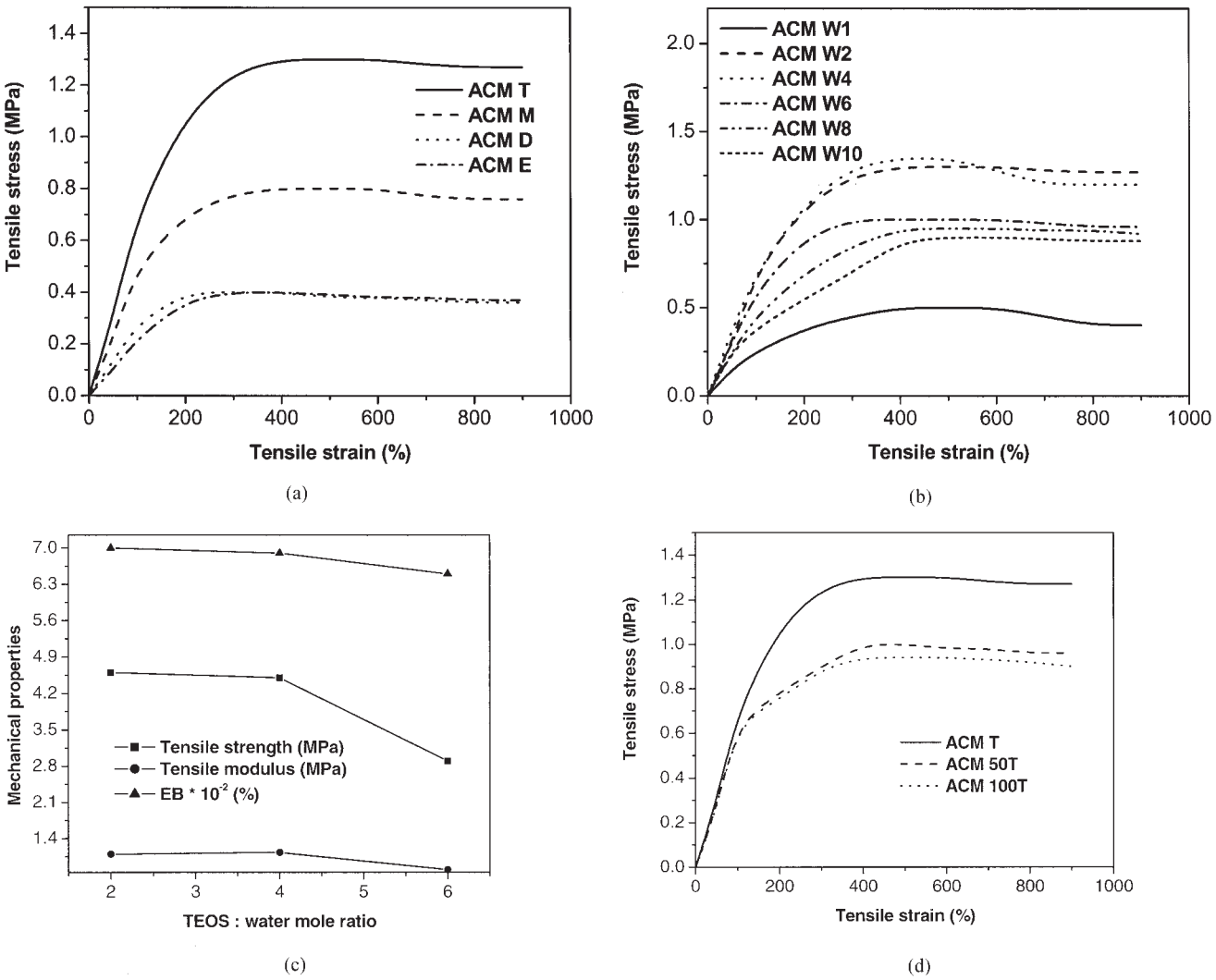

Figure 4 (a) Tensile stress–strain curves for uncured ACM/silica hybrid composites prepared from different solvents. (b) Tensile stress–strain plots for uncured ACM/silica hybrid composites prepared with different TEOS-to-water mole ratios. (c) Tensile strength, modulus (100%), and elongation at break (%) values for the representative cured ACM/silica hybrid composites prepared with varying TEOS-to-water mole ratios. (d) Tensile stress–strain plots for uncured ACM/silica hybrid composites prepared by varying the gelling temperature.

Studies on mechanical properties

Figure 4(a) shows the representative tensile stress–strain behavior of the uncured ACM/silica hybrid composites, prepared by using different solvents. The tensile strength of the uncured composites is calculated from the maximum stress values in the stress–strain curves. All the systems exhibit maximum stress at $\approx$ 300% elongation, after which the curves show a downward trend (i.e., yielding behavior). Maximum tensile strength and modulus (100%) are exhibited by ACM T and the least tensile strength and modulus are exhibited by ACM E and ACM D (Fig. 4(a) and Table VI). Tensile strength of the resultant composites decreases as the dielectric constant of the respective solvents (Tables I and VI) increases beyond that of THF. As discussed earlier, high polarity of the reaction medium may have caused greater solvation of the reactants, thereby restricting the silica generation within the hybrid composites prepared with more polar solvents compared to THF. For ACM E, although the polarity of the solvent is low, it does not mix with water appreciably. Therefore, it also shows less silica generation and the strength of the resultant composite is less. Despite the variation in strength, all the composites register very high elongation (>900%).

Figure 4(b) and Table VI report the tensile strength and the modulus of the uncured ACM/silica hybrid composites prepared by using different TEOS-to-water mole ratios. ACM W1 shows the lowest tensile strength and modulus compared to the other compositions. ACM W2 and ACM W4 show comparable strength and modulus values, although the former is

TABLE VI
Mechanical Properties Data for the Uncured Hybrid Composites

Composite designation	Tensile modulus at 100% elongation (MPa)	Tensile strength (MPa)	Elongation at break (%)
ACM T	0.70	1.30	>900
ACM M	0.50	0.80	>900
ACM D	0.28	0.40	>900
ACM E	0.22	0.40	>900
ACM W1	0.25	0.50	>900
ACM W2	0.70	1.30	>900
ACM W4	0.70	1.35	>900
ACM W6	0.59	1.00	>900
ACM W8	0.45	0.95	>900
ACM W10	0.38	0.88	>900
ACM 50T	0.65	0.98	>900
ACM 100T	0.65	0.78	>900

completely transparent, whereas the latter appears partially opaque. Partial opacity in the ACM W4 composite indicates local agglomeration of silica particles as observed in TEM photographs. These aggregations, however, have not reached the critical size to affect the mechanical properties. The composites (ACM W6–W10) containing higher proportions of water (higher than ACM W4) show lower strength, which decreases constantly with an increase in water content (i.e., ACM W6 > ACM W8 > ACM W10). Increasing the proportion of water causes more and more phase separation in the composites forming silica of larger size, which are not homogeneously dispersed like the nanosilica particles in ACM W1, ACM W2, and partially in ACM W4. The effective surface area provided for the polymer–filler interaction is likely to be reduced with the increasing size of the silica phase and, therefore, the tensile strength and the tensile modulus exhibit the decreasing trend. ACM W2 and ACM W4 give almost 185% improvement in tensile strength and modulus values compared to ACM W1 and there is $\approx$ 28% downfall in tensile strength for ACM W6. The tensile modulus of ACM W6 also decreases by 19% from the maximum value as observed in ACM W4.

The mechanical properties of the hybrids (ACM W2, ACM W4, and ACM W6, taken as representative) are further improved by curing the rubber phase, even though the extent of improvement is higher with the nanocomposites (ACM W2 and W4) compared to the microcomposites (ACM W6). Figure 4(c) depicts the tensile strength and the modulus values (100%) for the representative cured ACM/silica composites. The variation in strength of the composites is in line with the results obtained from the respective uncured composites. ACM W2 and ACM W4 give almost 247% improvement in tensile strength and 57% improvement in tensile modulus values over ACM W6. The transparent composite ACM W2 shows nanolevel dispersion of silica within the matrix, whereas ACM W4 shows partial opacity on account of the increased size of the silica particles. The improvement in strength and modulus are probably due to the synergism between the silica reinforcement and crosslinking of the rubber phase.[10] For ACM W6, the silica particles are bigger than those in ACM W4, which reduces filler–polymer interaction due to the decrease in effective surface area. It may have affected the ultimate tensile strength and tensile modulus due to these large particles acting as flaws and increasing stress concentration. The elongation at break value decreases with increasing the proportion of water in the composites. It is probably again due to the presence of silica agglomerates.

Figure 4(d) and Table VI report the mechanical properties of the uncured ACM/silica hybrid composites, prepared by varying the condensation temperature. The strength and modulus values decrease under accelerated condition (carried out at high temperature) from the ambient temperature values probably due to the formation of the silica agglomerates shown by TEM photograph. The composites still show very high elongation at break (>900%) probably due to the uncured nature of the matrix.

CONCLUSION

ACM/silica organic–inorganic hybrid composites with a fixed concentration of TEOS (45 wt %) were prepared by using the sol-gel technique. The pH of the medium was kept constant by adding an appropriate amount of concentrated HCl. The nature of the solvent, TEOS-to-water mole ratio, and temperature of the condensation reaction leading to the formation of silica was varied. Maximum silica generation was obtained in THF compared to the other solvents (MEK, DMF, and EAc) used under the same conditions of the reactions. The possible reason may be the optimum polarity of THF and its water miscibility. From the FTIR study, ACM E shows lower concentration of silica compared to other composites principally due to the nonuniform dispersion of the silica forming precursor. Formation of nanosilica within the hybrids is evident from the microscopic observations for the TEOS-to-water mole ratio up to 1:2, beyond which the agglomeration starts. ACM W1 shows low concentration (and dimension 25 nm) of the silica particles compared to ACM W2 (dimension 100 nm), which may be due to a lower extent of hydrolysis in the former. Hybrids containing higher water levels (1:8 and 1:10) delay gelation and are opaque in appearance. Existence of silica network is observed with TEOS-to-water mole ratio of 1:2, where the network-forming silica particles are apparently 90 nm in diameter. Aggregation of silica particles has also been observed with the

composites gelled at high temperature (50 and 100°C) compared to the ambient temperature. High silica concentration obtained through FTIR study (and also from the ash content data) with the increase in the water content in the hybrids was the result of the phase-separated morphology. The hybrids comprising bigger sized silica particles show lower mechanical reinforcement, as evident from the dynamic mechanical analysis. Higher T_g values along with the decrease in tan δ peak height have been noticed with the nanocomposites (ACM W2 and ACM W4), whereas the reverse phenomena is noted with the composites containing bigger silica particles. The nanocomposite exhibits superior mechanical properties (tensile strength and tensile modulus) compared to the microcomposites in both the cured and the uncured states. The possible reason may be the improper filler–polymer interaction due to the decrease in surface area and the presence of silica agglomerates that act as defects within the system. The crosslinked composites containing silica agglomerates also show lower elongations at break values.

References

1. Laine, R. M.; Sanchez, C.; Brinker, C. J.; Giannelis, E. P. Organic/Inorganic Hybrid Materials; Ed. Vol. 628, Warrendale, PA: Materials Research Society, 2000.
2. Sanchez, C.; Lebean, B. MRS Bull 2001, 26, 377.
3. Ogoshi, T.; Itoh, H.; Kim, K. M.; Chujo, Y. Macromolecules 2002, 35, 334.
4. Jiang, S.; Yu, D.; Ji, X.; An, L.; Jiang, B. Polymer 2000, 41, 2041.
5. Keeling-Tucker, T.; Rakic, M.; Spong, C.; Brennan, J. D. Chem Mater 2000, 12, 3695.
6. Gautier-Luneau, I.; Mosset, A.; Galy, J.; Schmidt, H. J Mater Sci 1990, 25, 3739.
7. Xie, T.; Zhou, C. G.; Feng, S. Y.; Wang, X. Q. J Appl Polym Sci 2000, 75, 379.
8. Juang Vanich, N.; Mauritz, K. A. J Appl Polym Sci 1998, 67, 1799.
9. Brinker, C. J.; Scherer, G. W. Sol-Gel Science: The Physics and Chemistry of Sol-Gel Processing, Academic Press: San Diego, CA, 1990.
10. Bandyopadhyay, A.; DeSarkar, M.; Bhowmick, A. K. Paper 43, Technical Meeting, Rubber Division, 14th–17th Oct 2003.
11. Bandyopadhyay, A.; DeSarkar, M.; Bhowmick, A. K. Communicated, 2004.
12. Bandyopadhyay, A.; DeSarkar, M.; Bhowmick, A. K. Communicated, 2004.
13. Jonas, J. Science of Ceramic Chemical Processing; Wiley: New York, 1986.
14. Orcel, G.; Hench, L. L. J Non-Cryst Solids 1986, 79, 177.